ELSEVIER

Nuclear Physics A 594 (1995) 375–405

NUCLEAR PHYSICS A

$\phi\pi^0$ and $\phi\eta$ production in antiproton annihilation at rest in a hydrogen gas target at NTP

V.G. Ableev [a,1], M. Agnello [b], F. Balestra [c], G. Bendiscioli [e], S. Bergamaschi [e], A. Bertin [f], E. Botta [c], T. Bressani [c], M. Bruschi [f], M.P. Bussa [c], L. Busso [c], D. Calvo [b], M. Capponi [f], C. Cavion [a], B. Cereda [f], P. Cerello [c], C. Cicalò [h], M. Corradini [d], S. Costa [c], S. De Castro [f], O.Yu. Denisov [g], F. D'Isep [c], A. Donzella [d], L. Fava [c], A. Feliciello [c], L. Ferrero [c], A. Filippi [c], V. Filippini [e], A. Fontana [e], D. Galli [f], R. Garfagnini [c], U. Gastaldi [a], B. Giacobbe [f], P. Gianotti [i], O.E. Gorchakov [g], A. Grasso [c], C. Guaraldo [i], F. Iazzi [b], A. Lanaro [i], E. Lodi Rizzini [d], M. Lombardi [a], V. Lucherini [i], A. Maggiora [c], S. Marcello [c], U. Marconi [f], G.V. Margagliotti [j], A. Masoni [h], B. Minetti [b], P. Montagna [e], M. Morando [k], F. Nichitiu [i,1], D. Panzieri [c], D. Parena [c], P. Pauli [j], C. Petrascu [i,2], M. Piccinini [f], S. Prakhov [g], G. Puddu [h], A. Rosca [i,2], E. Rossetto [c], A. Rotondi [e], A.M. Rozhdenstvensky [g], A. Saino [e], P. Salvini [e], L. Santi [l], M.G. Sapozhnikov [g], C. Scoglio [e], N. Semprini Cesari [f], S. Serci [h], R. Spighi [f], P. Temnikov [h], S. Tessaro [j], F. Tosello [c], V.I. Tretyak [g], G.L. Usai [h], L. Vannucci [a], S. Vecchi [f], G. Vedovato [a], L. Venturelli [d], M. Villa [f], A. Vitale [f], A. Zenoni [m,n], A. Zoccoli [f]

[a] *Laboratori Nazionali di Legnaro dell'INFN, I-35020 Legnaro (Padua), Italy*
[b] *Politecnico di Torino and INFN, Sezione di Torino, I-10125 Turin, Italy*
[c] *Istituto di Fisica, Universita' di Torino and INFN, Sezione di Torino, I-10125 Turin, Italy*
[d] *Dipartimento di Chimica e Fisica per i Materiali, Universita' di Brescia and INFN, Sezione di Torino, I-25060 Brescia, Italy*
[e] *Dipartimento di Fisica Nucleare e Teorica, Universita' di Pavia and INFN, Sezione di Pavia, I-27100 Pavia, Italy*

[1] On leave of absence from the Joint Institute for Nuclear Research, Dubna, SU-101 000 Moscow, Russia.
[2] On leave of absence from the Department of High Energy Physics, Institute of Atomic Physics, Bucharest, Romania.

SSDI 0375-9474(95)00345-2

[f] Dipartimento di Fisica, Universita' di Bologna and INFN, Sezione di Bologna, I-40100 Bologna, Italy
[g] Joint Institute for Nuclear Research, Dubna, SU-101 000 Moscow, Russia
[h] Dipartimento di Scienze Fisiche, Universita' di Cagliari and INFN, Sezione di Cagliari, I-09100 Cagliari, Italy
[i] Laboratori Nazionali di Frascati dell'INFN, I-00044 Frascati, Italy
[j] Istituto di Fisica, Universita' di Trieste and INFN, Sezione di Trieste, I-34127 Trieste, Italy
[k] Dipartimento di Fisica, Universita' di Padova and INFN, Sezione di Padova, I-35100 Padua, Italy
[l] Istituto di fisica, Universita' di Udine and INFN, Sezione di Trieste, I-33100 Udine, Italy
[m] Dipartimento di Chimica e Fisica per i Materiali, Universita' di Brescia, I-251060 Brescia, Italy
[n] INFN, Sezione di Pavia, I-27100 Pavia, Italy

Received 26 June 1995

Abstract

Data of antiproton annihilation at rest in a hydrogen gas target at NTP have been collected with the Obelix spectrometer exposed to the beam extracted from the LEAR accelerator of CERN. The reactions $\bar{p}p \to \phi\pi^0$ and $\bar{p}p \to \phi\eta$ have been studied. The analysis of the angular distribution of the kaons emitted by the ϕ decay has shown that the reaction $\bar{p}p \to \phi\pi^0$ occurs essentially from $^3S_1$ states with a production rate $R_{NTP} = (2.46 \pm 0.23 \pm 0.07) \times 10^{-4}$, while the rate from $^1P_1$ states is compatible with zero. Because of acceptance limitations, $^3S_1$ and $^1P_1$ contributions to the reaction $\bar{p}p \to \phi\eta$ could not be resolved and lower and upper limits for the production rate have been measured with the middle value $R_{NTP} = (0.87 \pm 0.21) \times 10^{-4}$. Also, for the phase-space $K^+K^-\eta$ events the production rate $R_{NTP} = (4.67 \pm 0.35) \times 10^{-4}$ has been measured. The $\phi\pi^0$ and $\phi\eta$ branching ratios in S- and P-waves (defined in the text) have been estimated in a model dependent way. For the evaluation of the $\phi\eta$ rate, a combination of our production rate and of data obtained with a liquid target has been used. The $\phi\pi^0$ production rate, compared to our preliminary value for the $\omega\pi^0$ production, confirms the strong violation of the OZI rule observed in other experiments. No violation is apparent in the $\phi\eta$ production.

1. Introduction

Significant violations of the Okubo–Zweig–Iizuka (OZI) rule [1] have been found recently in the antinucleon–nucleon annihilation at low energies [2–5]. According to the OZI rule, $\phi(1020)$ production is possible only if an admixture of u and d quarks exists in the ϕ wave function. The amount of this admixture is determined by the difference δ between the physical mixing angle θ and the ideal one $\theta_i \approx 35.3°$ [6]. If $\theta = \theta_i$, the ϕ-meson would be a pure $\bar{s}s$ state and its production in non-strange hadron interactions would be absolutely excluded by the OZI rule. However, vector mesons are almost ideally mixed and according to the quadratic Gell-Mann–Okubo mass formula the physical mixing angle is $\theta \approx 39°$ [6], hence $\delta \approx 3.7°$. The deviation from the OZI rule is measured through the parameter [7]

$$Z = \frac{M(A + B \to \bar{s}s + X)}{\left[M(A + B \to \bar{u}u + X) + M(A + B \to \bar{d}d + X)\right]/\sqrt{2}},$$

where the Ms are the amplitudes of the indicated reactions and A, B and X have no strange contents. Z can be evaluated through the ratio W between the production rate of the ϕ-meson and that of the ω-meson, which is an almost ideal admixture of $\bar{u}u$ and $\bar{d}d$ quarks. Z and W are correlated by the relation

$$W = \frac{R(A + B \to \phi X)}{R(A + B \to \omega X)} = \left(\frac{Z + \tan \delta}{1 - Z \tan \delta} \right)^2 F,$$

where F is a phase-space factor (typically $F \geqslant 1$). If the OZI rule is valid, then $Z = 0$ and for the production of ϕ and ω in the $\bar{p}p$ annihilation we expect

$$W_{OZI} = \frac{R(\bar{p}p \to \phi X)}{R(\bar{p}p \to \omega X)} = F \tan^2 \delta \approx 4.2 \times 10^{-3} F.$$

The OZI rule was tested in many reactions due to pp, πp and $\bar{p}p$ interaction at different energies, and in most of the cases the deviation from the OZI prediction was found to be quite low [7,8] (roughly, $|Z| \leqslant 0.1$ or $W/W_{OZI} \leqslant 10$). Surprisingly, in Refs. [2–5] very strong deviations are found, with $|Z| \approx 0.2$–0.5 and $W/W_{OZI} \approx 20$–60 (for a review see Ref. [9]).

The Asterix Collaboration [2] has measured the production rates $R(\phi X)$ with $X = \pi^0$, η, ω, ρ, $\pi^- \pi$ in $\bar{p}p$ annihilations at rest in a gas target at NTP. Combining under some simplifying assumptions measurements obtained in different conditions, they have carried out the branching ratios in pure S-and P-wave. Because of the direct connection with our work, it is worth giving some details of this analisys for the $\phi\pi^0$ production, as an example. The conservation of the G-, P- and C-parities restricts the possible quantum numbers of the $\bar{p}p$ system for the production of the $\phi\pi^0$ to the spin triplet $^{33}S_1$ state ($I^G J^{PC} = 1^+(1^{--})$) and to the spin singlet $^{31}P_1$ state ($I^G J^{PC} = 1^+(1^{+-})$). Ref. [2] has measured the rate of the above reaction using two samples of events characterised by different percentages of P-wave in the initial $\bar{p}p$ state: one collected in coincidence with L X-rays emitted in the cascade of the $\bar{p}p$ atom (92.5% P-wave) and one without coincidence (59% P-wave). Considering also the rate obtained with liquid hydrogen targets (mostly S-wave annihilations), it has been obtained by extrapolation that $\phi\pi^0$ is produced only in $^{33}S_1$ states (the branching ratio for pure P-wave turned out to be $(0.0 \pm 0.3) \times 10^{-4}$ and for pure S-wave $(4.0 \pm 0.8) \times 10^{-4}$).

Moreover, in Ref. [2] strong deviations from the OZI predictions have been observed only in S-wave annihilation channels, specifically for $X = \pi^0$ where $W/W_{OZI} \approx 20$ (in agreement with data obtained in liquid target [10]). No strong enhancement has been observed in P-wave. These results indicate a strong dependence of the OZI rule violation on the quantum numbers of the initial state.

The Crystal Barrel Collaboration [3] has measured $W = R(\phi X)/R(\omega X)$ for $X = \pi^0$, η, $\pi^0\pi^0$ and γ in $\bar{p}p$ annihilations at rest in liquid hydrogen. They have confirmed the Asterix observation of a large deviation from the OZI rule (1) for $X = \pi^0$, being $W = (96 \pm 15) \times 10^{-3}$. However, their most striking result is the extremely large ratio for $X = \gamma$, where $W = (243 \pm 86) \times 10^{-3}$, i.e. $W/W_{OZI} \approx 60$.

The Obelix Collaboration has measured $W = R(\phi X)/R(\omega X)$ in $\bar{n}$ annihilations in flight in liquid hydrogen [4] and has found $W = (110 \pm 15) \times 10^{-3}$ for $X = \pi^+$, i.e. $W/W_{OZI} \approx 25$. Also, a large enhancement above the OZI prediction has been found for $X = \pi^-$ ($W = (133 \pm 26) \times 10^{-3}$, i.e. $W/W_{OZI} \approx 30$) in $\bar{p}$ annihilations in gaseous deuterium [5].

So the very existence of the strong deviation from the OZI rule in the annihilation of low energy antinucleons is a firmly established experimental fact seen by different groups in different reactions.

A number of theoretical models [11–15] has been invoked for the explanation of these data. It is interesting that approaches based on the traditional conceptions [12–15] do not seem to be able to reproduce all features of the ϕ production. At the same time, unconventional ideas, like the polarised intrinsic strangeness in the nucleon [16,17], offer a rather natural explanation of the observed facts. However, additional detailed experimental studies of the ϕ production from different initial states into different final states are needed to clearly understand the physical reasons of the OZI violation.

This paper contributes to this research field with an experimental study of the reactions

$$\bar{p}p \to \phi\pi^0 \to K^+K^-\pi^0,$$
$$\bar{p}p \to \phi\eta \to K^+K^-\eta,$$

due to the $\bar{p}$ annihilation at rest in a hydrogen gas target at NTP. Notice that $\phi\eta$ may be produced in protonium levels with the same quantum numbers as for the $\phi\pi^0$ system (see above), except for the isospin and the G-parity which are 0^-, that is, in the levels with quantum numbers $^{13}S_1[0^-(1^{--})]$ and $^{11}P_1[0^-(1^{+-})]$.

2. Experimental conditions

The Obelix spectrometer is a detector system in a magnetic field (about 0.5 T) with a cylindrical symmetry around the beam line, which is parallel to the field axis (z axis of our reference system). The gas target was exposed to an antiproton beam (of 105 MeV/c momentum in the present measurement) extracted from the LEAR machine of CERN. With reference to Fig. 1, moving from the center, it is formed by a cylindrical gas target, a vertex detector, a first layer of scintillators for triggering purposes and time-of-flight measurements (called tofino), a jet drift chamber (JDC) for the tracking of the particles, a second layer of scintillators (called tofone) and an electromagnetic calorimeter for gamma-ray detection. The solid angle covered by the detectors is about 70% of 4π. A thin scintillator counter detects the beam, which is slowed down to stop in the middle region of the target. Detailed features and performances of the apparatus are described in Ref. [18].

The JDC and the two scintillator barrels (time-of-flight or TOF system) are the detectors utilised in the present analysis. The JDC measures the vertex coordinates of the events, the momentum of the particles and the specific energy loss ($-dE/dx$). TOF

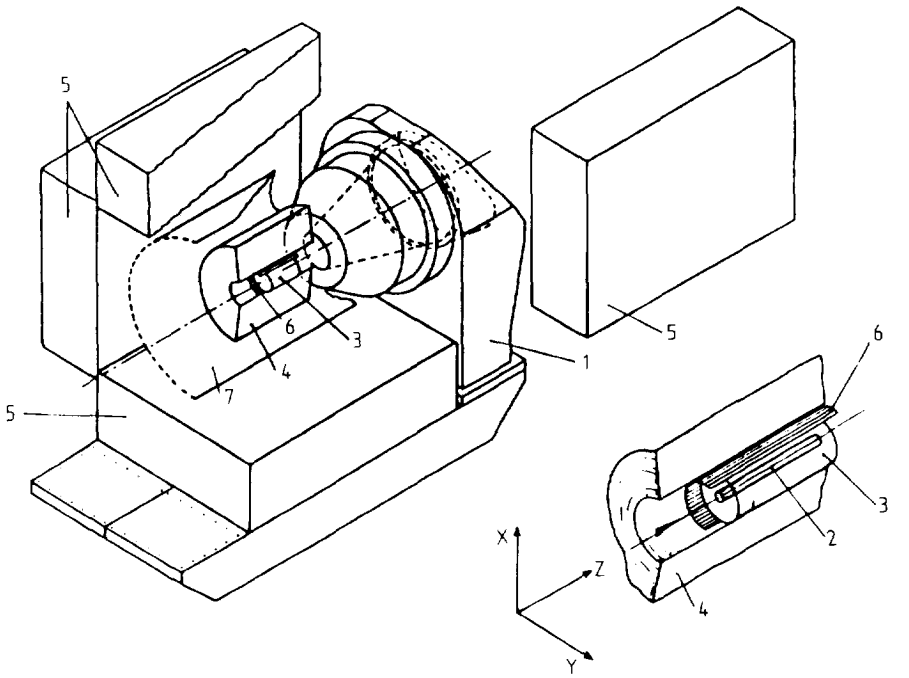

Fig. 1. Obelix spectrometer: view with a lateral supermodule of the EM calorimeter shifted in maintenance position. (1) Open field magnet; (2) target (diameter 6 cm, length 60 cm); (3) spiral projection chamber (SPC, external diameter 30 cm, length 60 cm, 90 sense wires); (4) jet drift chamber (JDC, internal diameter 40 cm, external diameter 160 cm, length 140 cm, 1722 sense wires, 41 azimuthal sectors of 4° for each chamber); (5) high angular resolution gamma-ray detector (HARGD, four supermodules $300 \times 400 \times 80$ cm^3 each). Time of flight system: (6) internal scintillator barrel (internal diameter 36 cm, thickness 1 cm, length 80 cm, 30 elements); (7) external scintillator barrel (internal diameter 270 cm, thickness 4 cm, 84 elements).

measures the time-of-flight and, together with the track length measured by the JDC, the velocity β.

Two distinct samples of events were recorded, one selected by trigger conditions requiring two hits in each scintillator barrel (two-prong trigger) and the other selected by the same trigger plus an additional trigger operating as follows (slow trigger). Annihilation kaons being on the average slower than pions, in order to increase the percentage of events with kaon production, events were recorded when the time difference between any hit in the inner scintillator barrel and the latest hit in the outer scintillator barrel was greater than 7 ns. According to a Monte Carlo simulation, this trigger condition increases the percentage of kaons by a factor of about 4, because typical pion time-of-flights are around 3 ns. The detection of slow particles has a limitation in the extreme low energy region due mainly to the material in the inner scintillator barrel: pions, kaons and protons with momenta lower than about 80, 200 and 300 MeV/c, respectively, cannot reach the JDC and be measured.

We collected a sample of 1.5×10^6 events with the simple two-prong trigger and a sample of 7.86×10^5 events with the slow particle trigger.

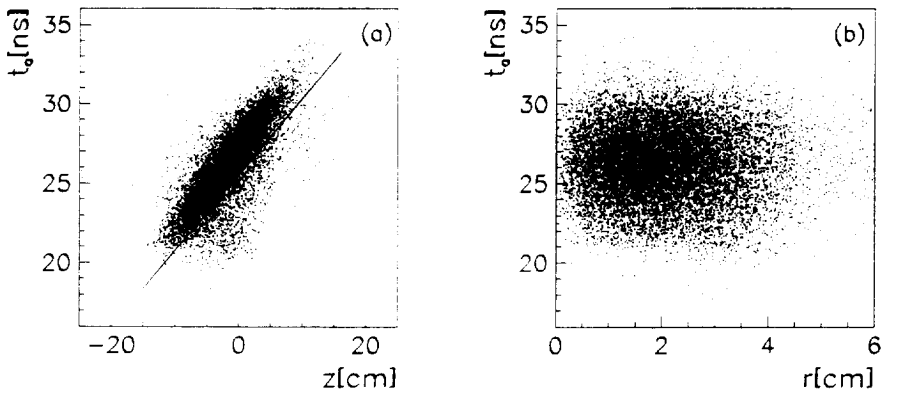

Fig. 2. (a) Annihilation time vs. the z vertex coordinate. (b) Annihilation time vs. the radial position r of the vertex. Events below the line in (a) (that is, with $t_a(\text{ns}) < 0.48\,z(\text{cm}) + 25.57$) *and* with $r > 2$ cm are neglected in the analysis (see text).

Antiprotons passing across the beam counter can annihilate in the front target window, in flight (negligibly) and at rest (mostly) in the gas target and in the cylindrical mylar wall of the target. In principle, the vertices of the annihilations in gas are spread in the central region of the target and have a radial position $r < 3$ cm, and those in the cylindrical mylar wall have $r = 3$ cm. Events in the target are identified through the position of their vertices and the annihilation time t_a determined by the first particle hitting the internal scintillator barrel, the $t_1 = 0$ time being fixed by the signal coming from the beam counter. Annihilation times of $\bar{p}$ stopped in the target and in the mylar walls are a function of the z vertex coordinate because of different $\bar{p}$ deceleration times and different deexcitation times of the antiprotonic atoms [19]. In particular, the electromagnetic cascade time of the antiprotonic atom lasts longer in gas than in the solid material of the wall: on the average, for hydrogen gas at NTP the difference between the two cascade times is of the order of a few ns [19–21]. Annihilations in flight are prompt. This allows us to reject most of the annihilations in flight and on the walls, simply recording only events with t_a greater than a minimum time. Fig. 2a shows the correlation between t_a and the z vertex coordinate, and Fig. 2b shows the correlation between t_a and the radial position r. Only events with $t_a > 21$ ns were recorded, which excludes most of the annihilations in the walls. Anyway, a number of target wall annihilations could still be present, because of the uncertainties on the vertex position and on the annihilation time. In order to eliminate them, we rejected events according to the annihilation time and the vertex position, as explained in the caption of Fig. 2. A similar selection is described, for instance, also in Ref. [22].

A sample of events was recorded without trigger selection (minimum bias events); events which should be selected by the triggers were labelled with a special flag. This sample allowed us to check the trigger efficiency and to include this information in the Monte Carlo simulation code.

The Monte Carlo simulation code generates events according to physical hypotheses and subjects them to the geometrical and energetic distortions caused by the interaction of the particles with the detectors, as in real events. In the simulation code, the geometry of the detectors, the materials, electromagnetic interactions, nuclear interactions, particle decays and any efficiency are taken into account. The code GEANT 3.21 was used in the Monte Carlo calculations.

The paper describes in detail the analysis of the slow particle trigger sample and gives only the final results on the other sample of ϕ events with lower statistics. The results are fairly consistent, which emphasises the reliability of our procedures.

3. Event selection

3.1. Introduction

Firstly, events have been selected with two prongs of opposite charge, with a vertex in the gas target as explained above and with tracks whose length projected on the plane perpendicular to the z axis is longer than 20 cm. These two-prong events include many final states. We mention (a) $\pi^+\pi^-\pi^+\pi^-\mathrm{n}\pi^0$, where a $\pi^+\pi^-$ pair was not seen because of the apparatus acceptance; (b) $\pi^+\pi^-\mathrm{n}\pi^0$; (c) $\mathrm{K}^+\mathrm{K}^-\mathrm{n}\pi^0$; (d) $\mathrm{K}^+\mathrm{K}^-\eta\mathrm{n}\pi^0$; (e) $\mathrm{K}^\pm\pi^\mp\mathrm{K}^0\mathrm{n}\pi^0$. Among them, the three-body final states $\mathrm{K}^+\mathrm{K}^-\pi^0$ and $\mathrm{K}^+\mathrm{K}^-\eta$ have been identified. Finally, the events produced via intermediate two-body states $\bar{\mathrm{p}}\mathrm{p}\to\phi\pi^0\to\mathrm{K}^+\mathrm{K}^-\pi^0$ and $\bar{\mathrm{p}}\mathrm{p}\to\phi\,\eta\to\mathrm{K}^+\mathrm{K}^-\eta$ have been picked up.

$\mathrm{K}^+\mathrm{K}^-\pi^0$ and $\mathrm{K}^+\mathrm{K}^-\eta$ events have been selected through the identification of the particles and kinematical fit procedures. Particles can be identified through two *independent* measurements: $-\mathrm{d}E/\mathrm{d}x$ (allowed by JDC) vs. momentum and the velocity $\beta = v/c$ (allowed by TOF) vs. momentum. For a number of tracks both measurements are possible, which permits a cross-check of the two ways. As a matter of fact, the energy loss measurement resulted to be effective in a higher number of tracks than the β measurement, and the latter resulted to be more selective in the high momentum region.

Fig. 3a shows the specific energy loss as a function of the momentum p. The $-\mathrm{d}E/\mathrm{d}x$ values accumulate along the theoretical curves given by the Bethe–Bloch formula. Most of the particles are π and K; their bands are distinguishable up to about 550 MeV/c. Fewer particles are protons: they are produced by the meson interaction with nuclei in the materials of the detectors, particularly in the scintillator barrels of tofino. Most of their tracks are not connected to the event vertices and do not affect the event analysis. A background of electrons and positrons (mixed with pions in the plot) is present in the minimum energy loss region. It is originated mainly by the interaction of γ-rays with tofino. Also these tracks are not connected to event vertices. Comments similar to the ones above hold for β as a function of the momentum p as shown in Fig. 3b. A noticeable difference is that the centers of the kaon and pion bands are still separated above a momentum of 550 MeV/c in the β plot, while they tend to overlap in the $-\mathrm{d}E/\mathrm{d}x$ plot.

3.2. Two-kaon-event selection

As most of the kaons due to ϕ decays have a momentum of less than 500 MeV/c (see, for instance, Fig. 14), we have based the two-kaon-event selection on the energy loss plot. Firstly, we considered events with both prongs belonging to the kaon band in the energy loss plot of Fig. 3a. Of course, not all the prongs in this band are kaons, particularly in the high momentum region.

For two-kaon events K^+K^-X, where X is anything recoiling against the kaons, the kinematics requires that the total momentum p_T and the invariant mass m_{KK} are related by the equation

$$p_T^2 = \left(\frac{4m_p^2 + m_{KK}^2 - m_X^2}{4m_p} \right)^2 - m_{KK}^2 ,$$

where m_X is the recoil mass. According to this equation, different types of events are arranged in specific ways in the (p_T, m_{KK}) plane (see Fig. 4a). In the case of no recoil particle ($p_T = 0$, $m_X = 0$), kaons fly back-to-back and the events are represented by the point ($p_T = 0$, $m_{KK} = 2m_p = 1876.5$ MeV/c^2). For fixed values of m_X or m_{KK}, the events are arranged along lines. For $m_{KK} = m_\phi$, the events are arranged along the vertical line with $m_{KK} = 1019$ MeV/c^2; for $m_X = m_\eta$ and $m_X = m_{\pi^0}$, the events are arranged along the lines labelled with η and π^0 in Fig. 4a. The $\phi\eta$ and $\phi\pi^0$ events are represented by the intersections between these lines and the previous straight line ($P_T = 500$ and 651 MeV/c, respectively). The multi-body events with $X = n\pi^0$ ($n \geqslant 2$) are spread quite uniformly in the region below the line for $m_X = m_{\pi^0}$; those with $X = \eta n\pi^0$ ($n \geqslant 1$) in the region below the line for $m_X = m_\eta$.

Fig. 4a shows that most of the measured events accumulate around the back-to-back point and along the η and π^0 lines with a background spread below the π^0 line, as

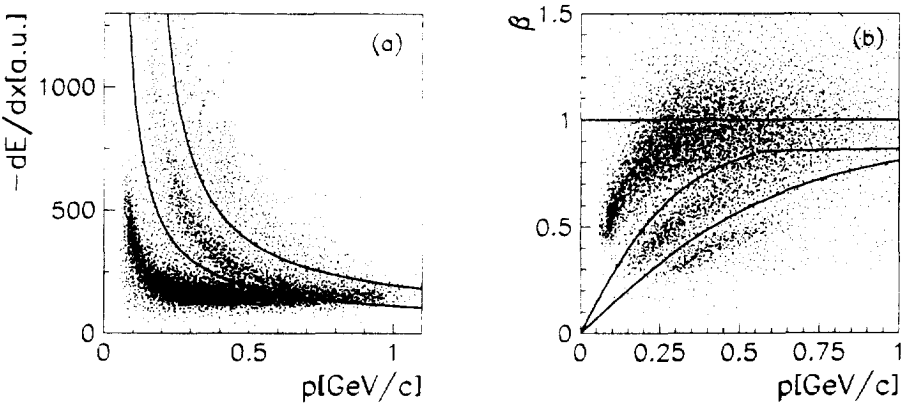

Fig. 3. (a) Distribution of the specific energy loss as a function of the momentum p for a sample of tracks. The momentum p is not measured at the vertex of the events, but in the JDC. Accumulation bands for π, K and p are clearly in evidence. The two lines define the kaon band (see text). (b) Distribution of the velocity β as a function of the momentum p for a sample of tracks. The kaon band is evidenced.

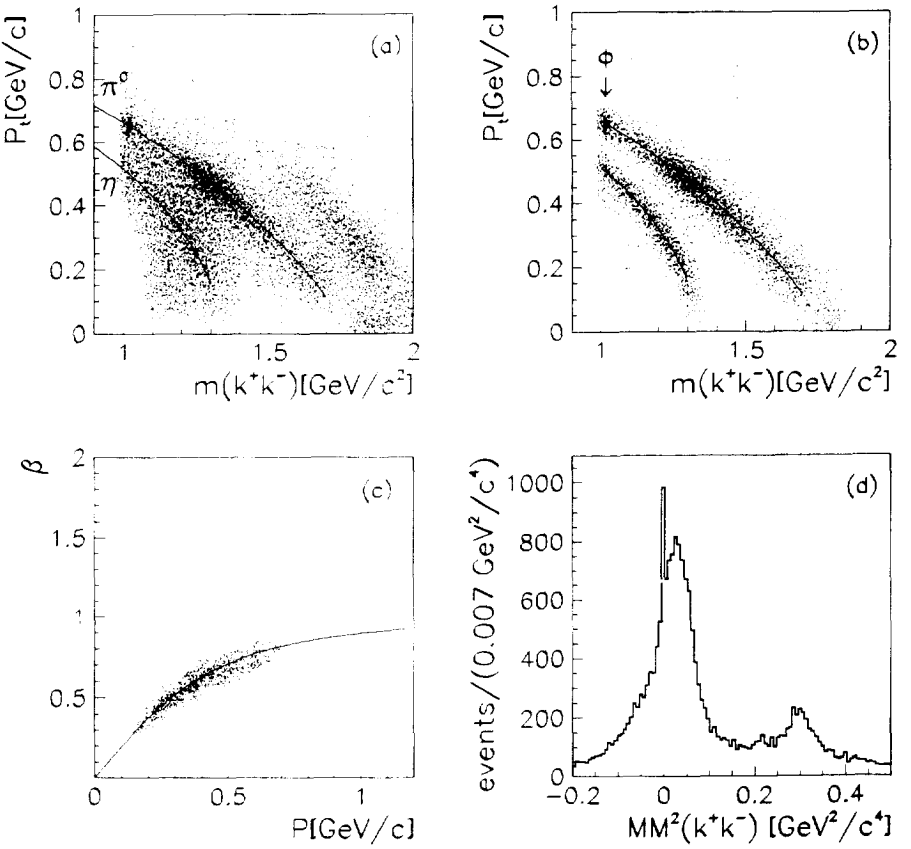

Fig. 4. (a) p_T vs. m_{KK} for events with two prongs belonging to the kaon band of Fig. 3a. Note the back-to-back events around ($p_T = 0$, $m_{KK} = 1876.5$ MeV/c^2), the events with the production of η (along the line on the left) and those with the production of π^0 (line on the right); ϕ spots are visible close to the upper limits of the two lines. Events accumulated above the back-to-back region are spurious (see text). Events spread far from the two lines have more than one neutral particle. Total number of events = 20686. (b) Events which have survived the kinematical fit to the reactions $K^+K^-\pi^0$ and $K^+K^-\eta$ (C.L. 95%). Total number of events = 8787. (c) β vs. p for a sample of tracks belonging to events selected in Fig. 4b. (d) Missing mass squared distribution of the events in Fig. 4a. The KK, $KK\pi^0$ and $KK\eta$ peaks are clearly seen.

expected; but there is also an accumulation of events in the unphysical region on the right side of the figure. These are spurious events, where real pions were treated as kaons: this occurs mainly for particles belonging to the high momentum region of the $(-dE/dx,\ p)$ diagram (see Fig. 3a), where the specific energy loss is less efficient for identifying particles. The E_T values of the spurious events are high (out of the physical region of Fig. 4a) as the kaon mass is higher than the pion mass. Of course, some events are spread in the unphysical region simply because of measurement errors. Note the ϕ accumulations at the upper end of the η and π^0 lines. Fig. 4d shows the missing mass squared distribution of the events in Fig. 4a; one can see distinct peaks corresponding to K^+K^-, $K^+K^-\pi^0$ and $K^+K^-\eta$ events on a smooth enough background due to reactions with X other than π^0 and η and events with the wrong kaon identification.

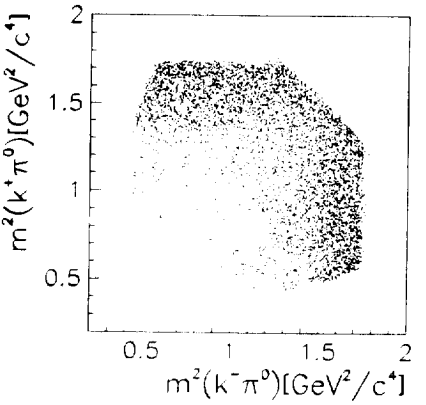

Fig. 5. Dalitz plot for $K^+K^-\pi^0$ phase space events according to a Monte Carlo simulation including the apparatus acceptance. $K^+\pi^0$ vs. $K^-\pi^0$ invariant mass squared.

The events filtered by the 1C kinematical fit to the reactions $\bar{p}p \to K^+K^-\pi^0$ and $\bar{p}p \to K^+K^-\eta$ (C.L. 95%) are shown in Fig. 4b; the corresponding missing mass distributions are given in Figs. 6a and 9a. The spread around the ideal lines indicates our resolution. The good selection of two kaon events through energy loss measurements and kinematical fits can be checked considering the tracks for which the β measurement has been possible (about $1/2$ of the tracks). We recall that the β measurement is independent of the energy loss measurement. Fig. 4c shows the behaviour of the velocity β as a function of the momentum p for kaons belonging to the events selected according to Fig. 4b. We may conclude that the contamination in Fig. 4b due to wrong identifications is negligible, and this is particularly true for the ϕ and $KK\eta$ regions.

3.3. Features of $K^+K^-\pi^0$

In order to introduce the analysis of the events selected according to Section 3.2, it is convenient to consider some features of phase space $K^+K^-\pi^0$ events, according to a Monte Carlo simulation (Fig. 5). Firstly, the size of the Dalitz plot is smaller than that of the undistorted phase space events due to the limitations in the detectable momenta. Then, the event density is not uniform, but decreases strongly while proceeding from the region of one or two slow kaons towards that of two fast kaons, as a consequence of the trigger selection.

The features of the data are displayed in Fig. 6a (missing mass squared distribution), Fig. 6b (Dalitz plot), Figs. 7a, 7b (K^+K^- invariant mass distribution), and Figs. 7c, 7d ($K^\pm\pi^0$ invariant mass distributions). The experimental Dalitz plot of Fig. 6b clearly shows a band corresponding to the ϕ resonance, an accumulation band due to the superimposition of the $f_2(1270)$ and $a_2(1320)$ resonances and two bands due to $K^{*\pm}$. Such bands are not displayed by the Monte Carlo phase space Dalitz plot. Fig. 7a shows the ϕ peak on the left side and the $f_2(1270)$ and $a_2(1320)$ resonances over a phase space

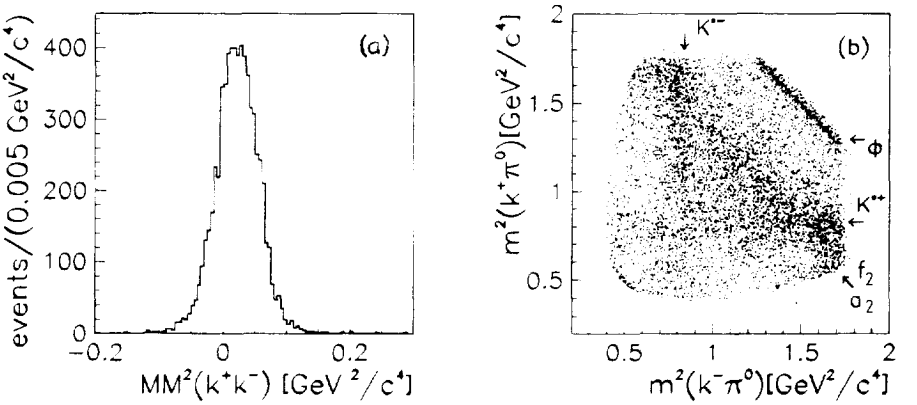

Fig. 6. Events filtered by the kinematical fit to the reaction $K^+K^-\pi^0$. (a) KK missing mass squared distribution. (b) Dalitz plot: $K^+\pi^0$ vs. $K^-\pi^0$ invariant mass squared. Total number of events = 6639.

background bump; the charged components of $a_2(1320)$ will be seen in Fig. 11. The small bump around 1625 MeV/c^2 is presumably a reflection of the $K^{*\pm}$ band crossing.

The main features of Figs. 6 and 7 change negligibly while slightly changing the event selection criteria (track length, kaon identification) and the cuts on the confidence level of the kinematical fits.

As an additional check of the correctness of the event selection, we considered false K^+K^- events. That is, we treated pairs of particles identified as $\pi^+\pi^-$, π^+K^- and π^-K^+ as if they were K^+K^-. Fractions of such events overcame the kinematical fit, but their Dalitz plots did not show any structure like that of the true K^+K^- events (see an example in Fig. 8).

3.4. Features of $K^+K^-\eta$

Figs. 9 and 10 show the results of the $K^+K^-\eta$ event selection. A spot in the Dalitz plot and a peak in the K^+K^- invariant mass distribution are a clear evidence of the ϕ resonance. No structures appear in the $K^\pm\eta$ invariant mass distributions. The size of the Dalitz plot is determined mainly by the "high" value of the η mass; cuts due to the apparatus acceptance are effective in the upper and right regions of the plot (slow kaons are not detected). We stress that the peak of fig. 10b includes two contributions, one due to the two-body final system $\phi\eta$ and the other due to the three-body system $\phi\pi^0\pi^0$, which cannot be separated by the kinematical fit. The peak is over a flat background due to $K^+K^-\eta$ and $K^+K^-\pi^0\pi^0$ events.

3.5. $K^\pm\pi^\mp K^0$

For the sake of completeness, we show in Fig. 11a the Dalitz plot for a sample of events with the production of $K^\pm\pi^\mp K^0$, selected with criteria similar to those previously described. In the plot the bands due to $K^{*\pm}$, K^{*0} and to the charged

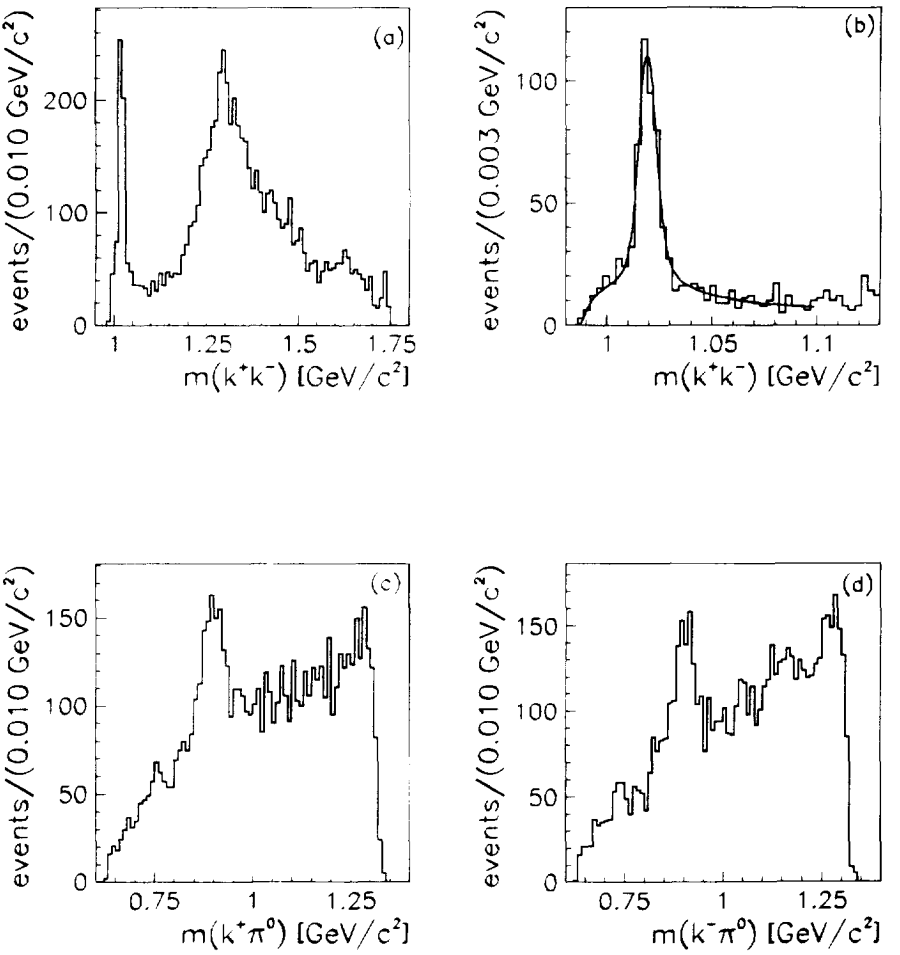

Fig. 7. Events filtered by the kinematical fit to the reaction $K^+ K^- \pi^0$. (a) $K^+ K^-$ invariant mass distribution. (b) Detail of (a). The best fit curve to the ϕ peak is shown (reduced $\chi^2 = 25/27$). (c) $K^+\pi^0$ invariant mass distribution. (d) $K^-\pi^0$ invariant mass distribution.

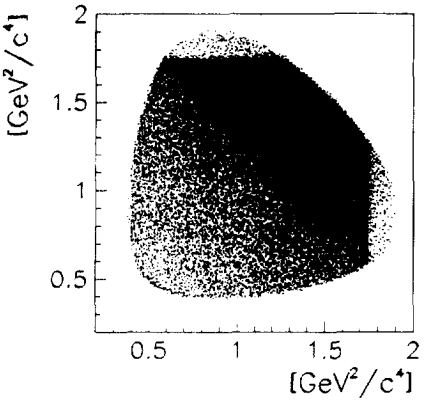

Fig. 8. Dalitz plot for false $K^+ K^- \pi^0$ events. $K^+\pi^0$ vs $K^-\pi^0$ invariant mass squared. In each event at least one particle is an identified pion (see text).

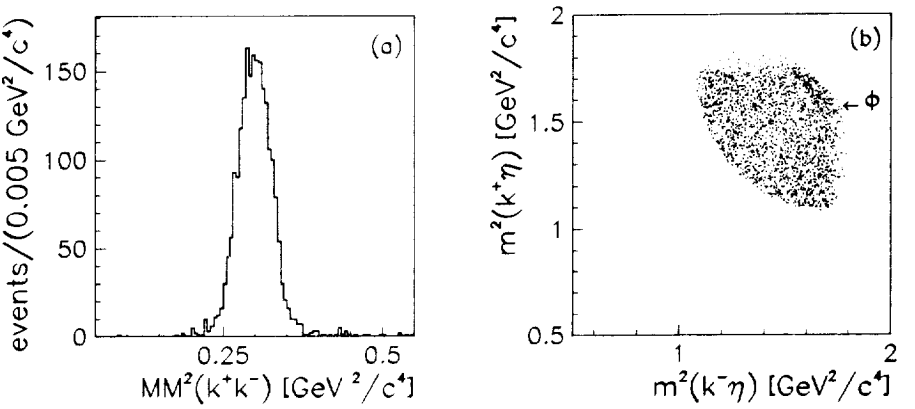

Fig. 9. Events filtered by the kinematical fit to the reaction $K^+K^-\eta$. (a) K^+K^- missing mass squared. (b) Dalitz plot: $K^+\eta$ vs. $K^-\eta$ invariant mass squared. Total number of events = 2171.

component of the $a_2(1320)$ resonance are clearly seen. Figs. 11b, 11c and 11d show the corresponding invariant mass distribuitions of the $K^0\pi^{\mp}$, $K^{\pm}K^0$ and $K^{\pm}\pi^{\mp}$ pairs, respectively.

3.6. Momentum distributions

$\phi\pi^0$ and $\phi\eta$ events are accumulated in peaks over a background as shown in Fig. 4a; Figs. 7b and 10b show their projection on the K^+K^- invariant mass axis (after kinematical fit selections). Anyway, the $\phi\pi^0$ and $\phi\eta$ signals can be evidenced with different criteria. For instance, one can consider the events (not filtered by kinematics fits) with an invariant mass within a narrow vertical band around the ϕ mass in Fig. 4a and build up their distribution as a function of p_T. For an invariant mass interval nearly as large as the ϕ peak, say

$$1.01 < m_{KK} < 1.03 \text{ GeV}/c^2.$$

the distribution of Fig. 12 is obtained. It displays a peak in the $\phi\eta$ region ($p_T = 500$ MeV/c) and one in the $\phi\pi^0$ region ($p_T = 651$ MeV/c). The η peak is due to two contributions: one coming from the two-body $\phi\eta$ events and the other from the phase space $K^+K^-\eta$ events. Similarly, the π^0 peak includes $\phi\pi^0$ and $K^+K^-\pi^0$ contributions. The peaks emerge over a smooth background due mainly to $\phi n\pi^0$ and $K^+K^-n\pi^0$ events, which becomes negligible under the π^0 peak. We stress that the $K^+K^-\eta$ and $K^+K^-\pi^0$ events are accumulated in peaks as the distribution is obtained by projecting on the p_T axis only the events belonging to a narrow m_{KK} interval whose width is comparable to the ϕ width (see Fig. 4a).

The momentum distributions are more regular than the invariant mass distribution, as they are not depleted by the kinematical fit selections, and turn out to be more suitable to evaluate the production rate of $\phi\eta$ events, whose statistics is poor (Section 5.3.1).

4. S- and P-wave contribution to the $\phi\pi^0$ production

In order to extract the contributions from S- and P-waves, we have taken advantage of the different angular and momentum features of the $K^+K^-\pi^0$ decays from $^3S_1$ and $^1P_1$ states. We indicate with θ the angle between the momentum of a (positive) kaon emitted by ϕ and the π^0 momentum in the ϕ center-of-mass system (see Fig. 13). The angular distributions for the $^3S_1$ and $^1P_1$ states, respectively, are [23]

$$d_S = \sin^2\theta,$$

$$d_P = 1 + (p^2/s)\cos^2\theta,$$

where $s^{1/2}$ is the total energy, $p^2 = [(s - m_\phi^2 - m_{\pi^0}^2)/2m_\phi]^2 - m_{\pi^0}^2$ and $p^2/s = 0.41$.

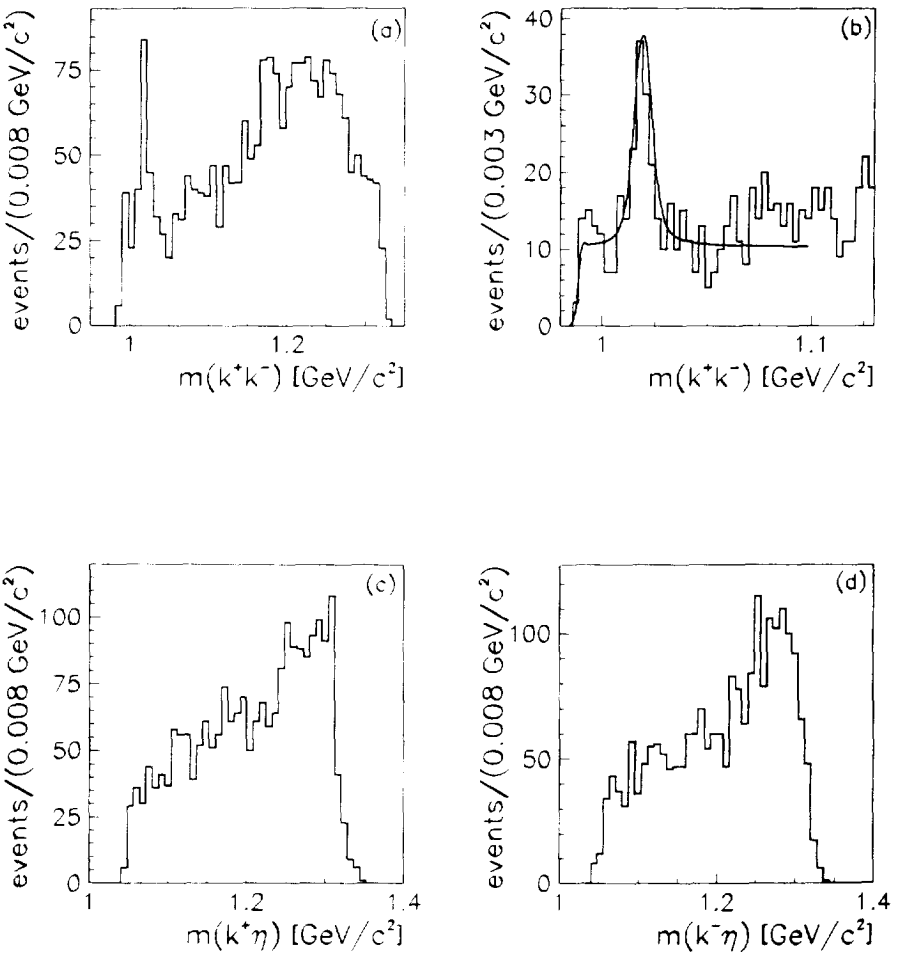

Fig. 10. Events filtered by the kinematical fit to the reaction $K^+K^-\eta$. (a) K^+K^- invariant mass distribution. (b) Detail of (a). The best fit curve to the ϕ peak is shown. (c) $K^+\eta$ invariant mass distribution. (d) $K^-\eta$ invariant mass distribution.

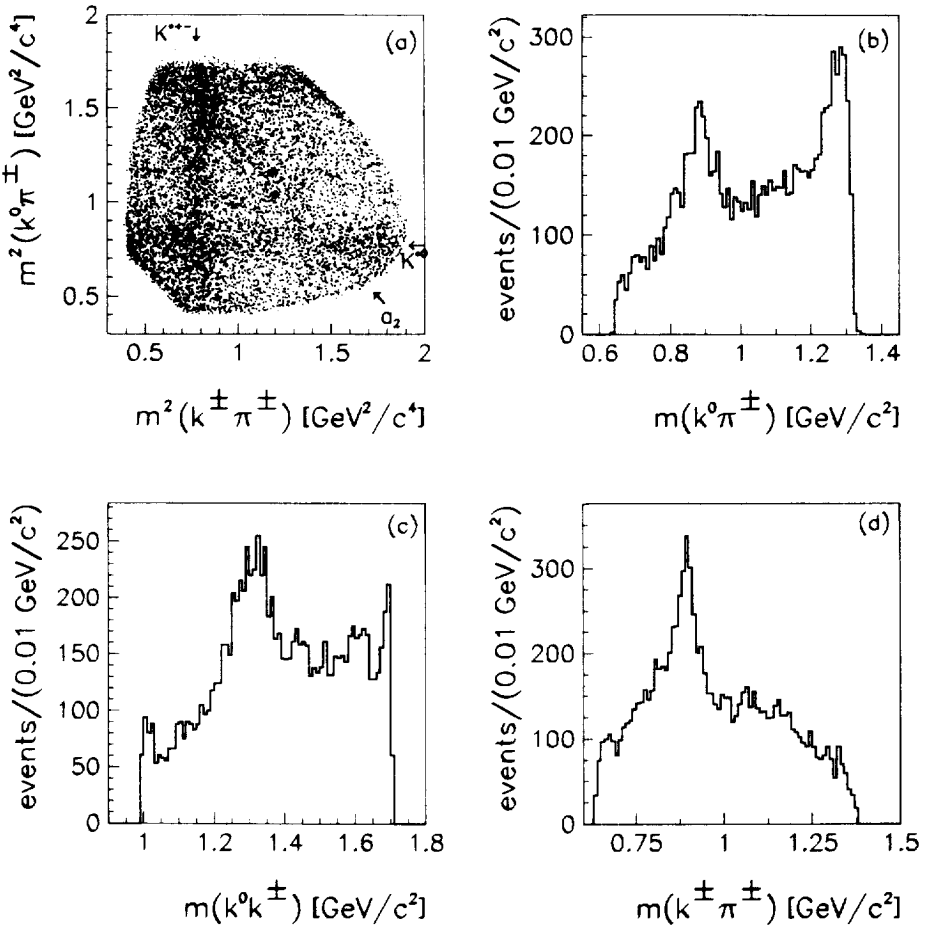

Fig. 11. (a) Dalitz plot for $K^+K^0\pi^-$ events: $K^0\pi^-$ vs. $K^+\pi^+$ invariant mass squared. Total number of events = 10182. (b) $K^0\pi^-$ invariant mass distribution. Note the $K^{*\pm}$ peak. (c) $K^\pm K^0$ invariant mass distribution. Note the $a_2(1230)$ peak. (d) $K^+\pi^-$ invariant mass distribution. Note the K^{*0} peak.

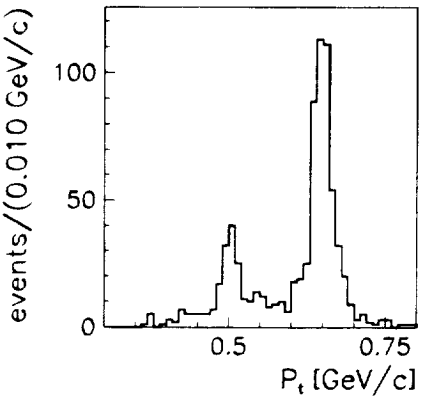

Fig. 12. p_T distribution for K^-K^- pairs in the invariant mass interval 1.01–1.03 GeV/c^2 around the ϕ peak.

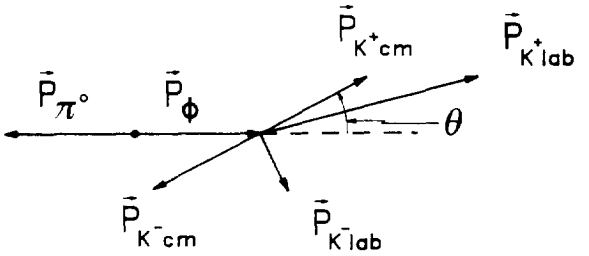

Fig. 13. Definition of the θ angle.

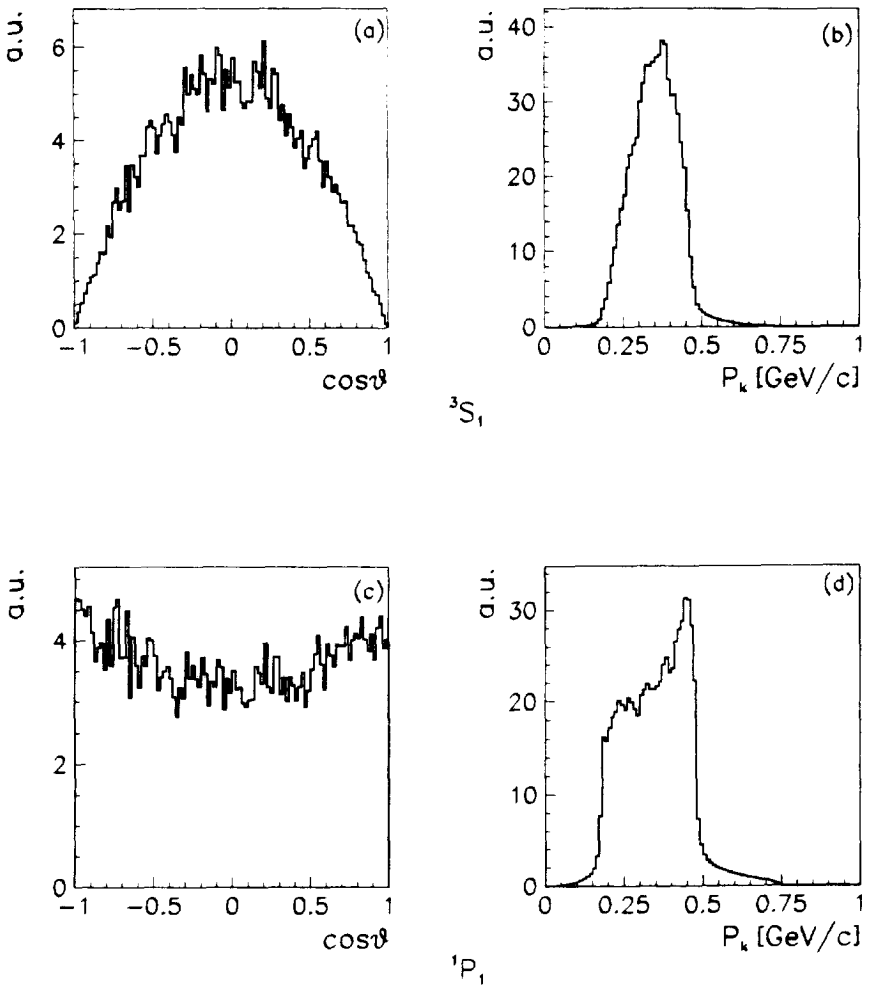

Fig. 14. Features of $\phi\pi^0$ events without distortions due to the apparatus acceptance. $^3S_1$ initial state: (a) cos θ distribution; (b) p_K distribution. $^1P_1$ initial state: (c) cos θ distribution; (d) p_K distribution.

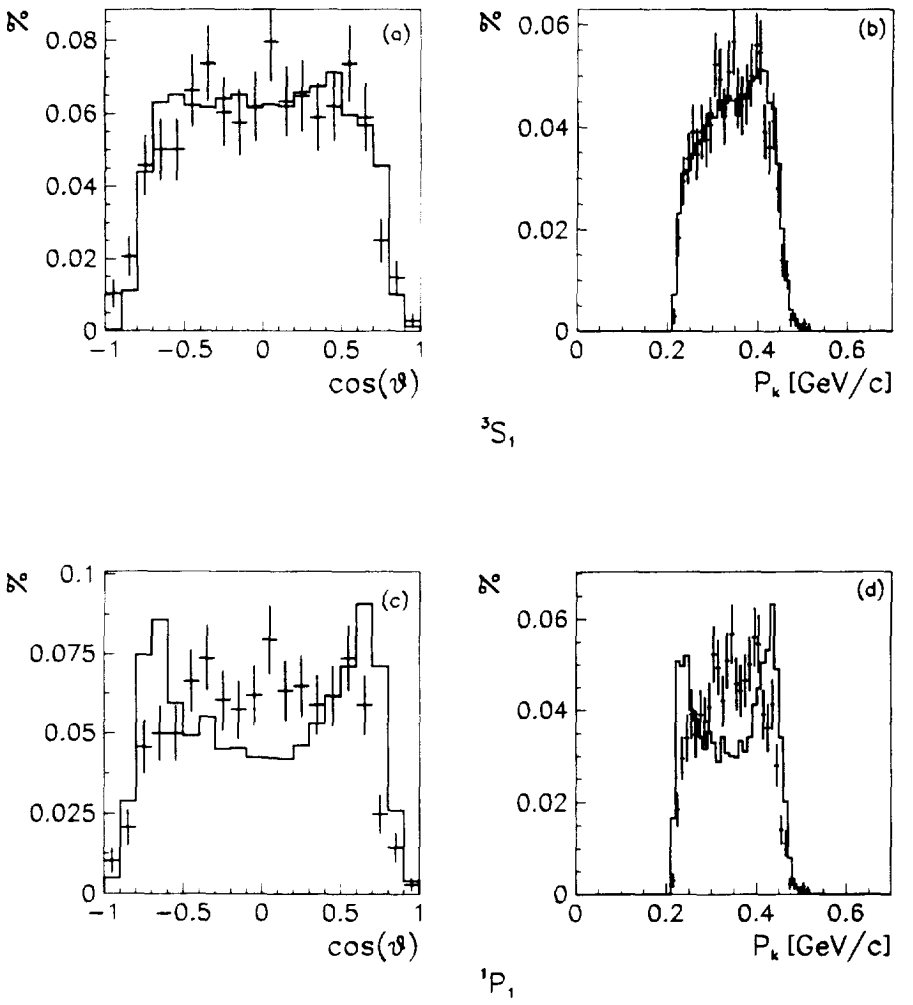

Fig. 15. S-wave $\phi\pi^0$: (a) cos θ distribution; (b) p_K distribution. P-wave $\phi\pi^0$: (c) cos θ distribution; (d) p_K distribution. Histograms from Monte Carlo simulations for pure S- and P-wave annihilations, crosses from the experiment.

The cos θ and momentum distributions for the S- and P-wave without the distortions due to the apparatus acceptance are shown in Fig. 14. Fig. 15 compares the experimental distributions (crosses) with Monte Carlo simulations (histograms).

We have fitted the experimental angular distribution by an admixture of pure P- and S-wave distributions with weights to be determined by the fitting procedure. We notice that the detection and measurement efficiencies are somewhat different for the S- and the P-wave because of the different kaon angular distributions (about 4.5% against 4%). The $K^+K^-\pi^0$ events within the interval $|m_\phi - m_{KK}| < 10$ MeV/c^2 in Fig. 7b have been selected. The best fit procedure has indicated that $\phi\pi^0$ are produced essentially in S-wave; indeed the found percentage of S-wave is $R_S(\phi\pi^0) = (100 \pm 13)\%$, hence

$$R_P(\phi\pi^0) = (0 \pm 13)\%.$$

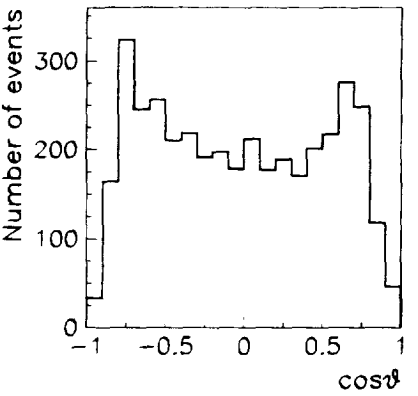

Fig. 16. cos θ distribution for false $K^+K^-\pi^0$ events. The particles were not identified, so that they are mostly pions. The distribution looks like a P-wave distribution rather than an S-wave one.

in agreement with Ref. [2]. Of course, a very small contribution from a P-wave cannot be excluded, but it cannot be detected with our statistics.

In the above invariant mass interval under the ϕ peak there is about 20% of background events, but they affect the above result negligibly in the limit of our statistics. To check this, we have considered different intervals of the KK invariant mass distribution around the ϕ peak and observed that the wider the interval (i.e., the higher the fraction of background), the lower the percentage of S-wave appears. Moreover, we have changed somewhat the particle identification criteria, obtaining samples of events with reduced background in the same invariant mass interval as above and obtaining values of R_S consistent with the above one; for instance, with a background of 12% we found $R_S(\phi\pi^0) = (90 \pm 13)\%$. Finally, we have found that the cos θ distributions of false $\phi\pi^0$ events (see Section 3.3) are very different from those of the true events (compare Fig. 16 with Fig. 15).

An analysis like the one above is not practicable for the $\phi\eta$ events as the η mass is higher than the π^0 mass; consequently, the mean kaon momentum in the laboratory system is smaller and the effects of the limited acceptance of our apparatus in the low momentum region are heavier than in the $\phi\pi^0$ case. In particular, the S- and P-wave angular distributions are very distorted close to cos $\theta = \pm 1$ and appear to be indistinguishable.

5. Evaluation of the production rates at NTP and estimation of the branching ratios

The frequency or production rate of the reaction $\bar{p}p \to \phi X$ ($X = \pi^0, \eta$) can be written in the form [24–26]

$$R_T(\phi X) = (1 - P_T) F_{TS} B_S(\phi X) + P_T F_{TP} B_P(\phi X),$$

where S and P stand for $^3S_1$ and $^1P_1$, respectively, P_T is the percentage of annihilations in P-wave and $(1-P_T)$ that in S-wave, F_{TS} and F_{TP} are, respectively, the percentages of S and P annihilations in the substates $^3S_1$ and $^1P_1$; $P_T F_{TP}$ is the *annihilation fraction* F_{1+-} as defined in Ref. [26]. The quantities B_S and B_P are the *intrinsic* branching ratios which describe the annihilation dynamics. P_T and F_{Ti} depend on the target density and the label T indicates the type of hydrogen target (liquid, NTP gas, etc.). As the F_{Ti} are unknown, we define the quantities $BR_i^T(\phi X) = F_{Ti} B_i(\phi X)$, which are target dependent in principle. We will call them experimental branching ratios or simply branching ratios. Usually people make the tacit, although arbitrary, assumption that the F_{Ti} are target independent: in our case, this means $F_{NTP}(^3S_1) = F_L(^3S_1)$ and $F_{NTP}(^1P_1) = F_L(^1P_1)$. Consequently, also the experimental branching ratios are target independent. Later, we also will resort to this approximation.

In terms of experimental branching ratios the above relation becomes

$$R_T(\phi X) = R_{TS}(\phi X) + R_{TP}(\phi X) = (1-P_T)\ BR_S^T(\phi X) + P_T\ BR_P^T(\phi X). \tag{1}$$

The number of detected events for a channel ϕX is related to the production rates and to the branching ratios through the relation

$$\begin{aligned} N_{\phi X} &= N_{\bar{p}}\varepsilon\left[(1-P_T)\ BR_S^T(\phi X)\varepsilon_{\phi XS} + P_T\ BR_P^T(\phi X)\varepsilon_{\phi XP}\right] \\ &= N_{\bar{p}}\varepsilon\left[R_{TS}(\phi X)\varepsilon_{\phi XS} + R_{TP}(\phi X)\varepsilon_{\phi XP}\right], \end{aligned} \tag{2}$$

where $N_{\bar{p}}$ is the number of antiprotons stopped in the target, $\varepsilon_{\phi XS}$ and $\varepsilon_{\phi XP}$ are the detection and reconstruction efficiencies for events produced in S- and P-waves, $\varepsilon = \varepsilon(\phi \to K^+K^-)$ is the decay rate of ϕ into charged kaons. $\varepsilon_{\phi XS}$ is defined as

$$\varepsilon_{\phi XS} = N_{\phi XS}(\text{reconstructed})/N_{\phi XS}(\text{generated}),$$

and its value is determined by Monte Carlo simulations. A similar definition holds for $\varepsilon_{\phi XP}$. Our results on production rates and branching ratios are summarised and compared with those from other experiments in Table 1 and Fig. 19.

5.1. Number of incident antiprotons

The total number of antiprotons stopped in the gas target is basically determined by the number N_{ch} of coincidences between the beam detector signals and the signals from the inner barrel of the TOF system within the time gate; this is the number of annihilations with at least one detected charged prong. It must be corrected for a number of factors. First, the event acquisition is inhibited each time an incident antiproton comes too close in time to the previous one; the number of unrecorded events must be subtracted. Then, we have to add a number of annihilations into neutrals, to subtract the number of those in the mylar wall of the target (see Section 2) and to take into account the efficiency of tofino (number of signals over the number of hitting particles). Annihilations into charged particles moving outside the solid angle covered by tofino and annihilations in flight are negligible. Finally, the number of stopped antiprotons is

$$N_{\bar{p}} = N_{ch}(1-R_1)(1-R_2)(1+R_0)/\varepsilon_1,$$

Table 1
Experimental results of production rate (R) and branching ratio (BR) for $\phi\pi^0$ and $\phi\eta$ production in units of 10^{-4}

	Parameter	Value ($\times 10^{-4}$)	Hydrogen target	Reference
$\phi\pi^0$	R	$2.46 \pm 0.23 \pm 0.07$	gas NTP	this experiment
	R	1.9 ± 0.5	gas NTP	[2]
	R	0.3 ± 0.3	gas NTP, X-ray	[2] [a]
	R	5.5 ± 0.7	liquid	[31]
	R	3.0 ± 0.3	liquid	[10]
	BR	4.0 ± 0.8	$^3S_1$	[2]
	BR	$5.22 \pm 0.48 \pm 0.56$	$^3S_1$	this experiment
	BR	0 ± 0.3	$^1P_1$	[2]
	BR	0 ± 0.7	$^1P_1$	this experiment
$\phi\eta$	R	$0.74 \pm 0.22 \pm 0.03$	gas NTP, lower limit [b]	this experiment
	R	$1.04 \pm 0.33 \pm 0.05$	gas NTP, upper limit [b]	this experiment
	R	0.87 ± 0.21	gas NTP [c]	this experiment
	R	0.37 ± 0.09	gas NTP	[2]
	R	0.41 ± 0.16	gas NTP, X-ray	[2] [a]
	R	0.66 ± 0.19	liquid	[3]
	R	0.48 ± 0.17	liquid	[34] [d]
	BR	0.30 ± 0.39	$^3S_1$	[2]
	BR	0.64 ± 0.25	$^3S_1$	this experiment [e]
	BR	0.42 ± 0.20	$^1P_1$	[2]
	BR	1.18 ± 0.84	$^1P_1$	this experiment [e]
$K^+K^-\eta$	R	4.67 ± 0.35	gas NTP	this experiment
$BR(\phi\pi^0)/BR(\phi\eta)$		$8.3 \pm 1.7 \pm 1.3$	liquid	[34]

[a] Data collected in coincidence with L X-rays emitted from the antiprotonic atom.
[b] These values are lower and upper limits of the production rate evaluated under the assumption that the $\phi\eta$ production occurs all in S-wave or all in P-wave.
[c] Average production rate evaluated assuming $BR_S = BR_P$ in Eq. (2).
[d] Deduced from the value of $BR(\phi\pi^0)/BR(\phi\eta)$ in a liquid target from Ref. [34] and $BR_S(\phi\pi^0)$ from Ref. [2].
[e] Deduced from NTP gas and liquid target data (see Section 5.3.1).

where ε_t is the efficiency of tofino, R_1 is the fraction of unrecorded events, R_2 is the fraction of events with the vertex on the mylar wall of the target, and R_0 is the percentage of annihilations which produce no signal in the internal scintillator barrel; they include both neutral channels and charged channels with the charged particles escaping the solid angle covered by the apparatus. R_0 was evaluated in a previous measurement of the reaction $\bar{p}p \to \pi^0\pi^0$ [27]. (It is worthwhile noting that the found value (see below) is comparable with the fraction of annihilations into neutrals measured in the NTP gas target [28] $(2.9 \pm 0.5)\%$, and in the liquid target, $(4.1^{+0.2}_{-0.6})\%$ [29]). Considering the numbers:

$N_{ch} = 91\,011\,623$,
$R_1 = 0.11708 \pm 0.00092$,
$R_2 = 0.07212 \pm 0.00043$,
$R_0 = (2.77 \pm 0.03 \pm 0.03)\%$,
$\varepsilon_t = 0.959 \pm 0.001$,

we have

$$N_{\bar{p}} = (7.99 \pm 0.01) \times 10^7.$$

5.2. $\phi\pi^0$ production

5.2.1. Evaluation of $N_{\phi\pi^0}$

In order to evaluate $N_{\phi\pi^0}$, we may consider the KK invariant mass distribution (Fig. 7b) or the p_T distribution (Fig. 12). Of course, the result is independent of the procedure, as we have checked. Here we use the invariant mass distribution. The ϕ peak emerges sharply from a background due to the phase space KK invariant mass distribution, which is flat in the ϕ region, and to the tails of the resonances $a_0(980)$ and $f_0(975)$, which have full widths of the order of 50 MeV. In order to get the number of events $N_{\phi\pi^0}$, the experimental distribution of the KK invariant mass in the ϕ region has been fitted with the following function ($m = m_{KK}$):

$$f(m) = Af_\phi + Bf_{bg} + Cf_{a_0},$$

where

$$f_\phi = (BW_\phi * G)(a + bm + cm^2 + dm^3)$$

describes the ϕ peak and its integral gives N_ϕ; BW_ϕ is the Breit–Wigner function for the ideal ϕ peak [23,30]:

$$BW_\phi = \frac{\Gamma(m)}{\left(m_\phi^2 - m^2\right)^2 + \Gamma^2(m)m_\phi^2},$$

$$\Gamma(m) = \Gamma_\phi \left(\frac{q(m)}{q(m_\phi)}\right)^3 \frac{m_\phi}{m},$$

where $\Gamma_\phi = 4.43$ MeV is the nominal resonance width, $q(m)$ is the relative momentum of the two kaons produced by the ϕ decay and m the relevant invariant mass. $(BW_\phi * G)$ is the convolution between BW_ϕ and a gaussian G, the σ of which takes into account the measurement errors. G and the third order polynomial take into account any effects depending on the apparatus. The values of the parameters $(\sigma, a, \ldots, d)$ were determined by fitting f_ϕ to the invariant mass distribution for $\phi\pi^0 \to K^+K^-\pi^0$ obtained with a Monte Carlo simulation (see Fig. 17). m_ϕ and Γ were fixed at the standard values [6].

The background function f_{bg} was assumed to have the form

$$f_{bg}(m) = 1 - \exp[-h(m - m_{th})],$$

where $m_{th} = 2m_{K^+} = 986$ MeV/c^2 is the energy threshold of the invariant mass distribution. h was determined by fitting this function to the phase space invariant mass distribution.

$f_{a_0}(m)$ is the convolution of a Breit–Wigner function and a gaussian with the same σ as for ϕ, which describes the tail of the a_0 resonance.

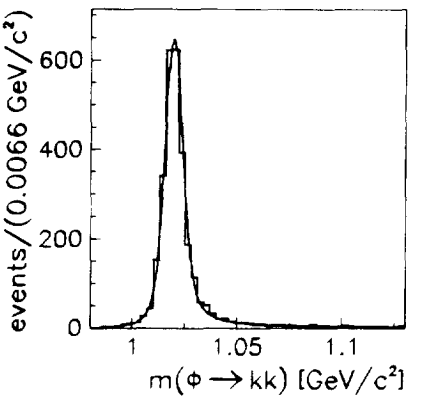

Fig. 17. Reaction $\bar{p}p \to K^+ K^- \pi^0$, $K^+ K^-$ invariant mass distribution. Monte Carlo simulation of the $K^+ K^-$ invariant mass distribution for the reaction $\bar{p}p \to \phi\pi^0 \to K^+ K^- \pi^0$ and best fit function (see text, reduced $\chi^2 = 30.6/25$).

With the above choice for $f(m)$ we have minimised arbitrary assumptions which could lead to unreliable values of N_ϕ. In the best fit procedure at a first approach the only free parameters were A, B and C; then also other parameters, such as σ and m_ϕ, were allowed to change in order to get a reduced χ^2 the closest to 1 (see Fig. 7b). We have fitted the data integrating $f(m)$ in each bin of the experimental histogram. The final invariant mass resolution turned out to be $\sigma = 3.20 \pm 0.03$ MeV/c^2. This final value is very close to the initial one (given by a Monte Carlo simulation) as well as that the final m_ϕ value is very close to the standard one (1019.4 MeV/c^2). The total number of events resulted to be 434 ± 40.

5.2.2. Evaluation of $R_{NTP}(\phi\pi^0)$

As the $\phi\pi^0$ production in P-wave is negligible (Section 4 and Ref. [2]), taking into account the measured quantities:

$$N_{\phi\pi^0} = 434 \pm 40,$$

$$\varepsilon_{\phi\pi^0 S} = (4.49 \pm 0.11) \times 10^{-2},$$

and the known quantity

$$\varepsilon(\phi \to K^+ K^-) = (49.1 \pm 0.8) \times 10^{-2},$$

we obtained by Eq. (2)

$$R_{NTP}(\phi\pi^0) = R_{NTPS}(\phi\pi^0) = N_{\phi\pi^0}/\varepsilon N_{\bar{p}} \varepsilon_{\phi\pi^0 S} = (2.46 \pm 0.23 \pm 0.07) \times 10^{-4},$$

where the former error is "statistical" (it originates from $N_{\phi\pi^0}$) and the latter is systematic (it is a quadratic combination of the errors on $N_{\bar{p}}$ and on the other quantities).

Actually, the former error is not a pure statistical error as it does not depend on the number of events only, but also on the procedure followed to separate the signals from the background. $R_{\rm NTP}(\phi\pi^0)$ has been evaluated also with somewhat different event selection criteria and with different shapes for $f(m)$; the results are very close to that quoted above.

The $\phi\pi^0$ production rate has been measured in three other experiments. With a NTP gas target the Asterix Collaboration [2] has found $(1.9 \pm 0.5) \times 10^{-4}$; with the same target and with L X-rays in coincidence they have found a value compatible with zero, $(0.3 \pm 0.3) \times 10^{-4}$. These values are in agreement with ours, but our error in $R_{\rm NTP}$ is smaller by a factor of about 2. With a liquid target there are two measurements with values higher than those in gas: $(3.0 \pm 1.5) \times 10^{-4}$ and $(5.5 \pm 0.7) \times 10^{-4}$ (Refs. [10,31], respectively). In spite of the uncertainties on the above values, we may conclude as follows. If $\phi\pi^0$ is produced only (or mainly) in S-wave, one expects that the production rate increases while increasing the target density and decreases when L X-rays are requested in coincidence: these expectations are confirmed by comparing the above values obtained in different conditions. The consistency of this picture suggests that the ensemble of these three measurements is not plagued by large systematic errors. Since the channel is produced only from $^3S_1$ states for dynamical reasons, the measurement of $R(\phi\pi^0)$ provides in a model independent way a quantity proportional to the 1^{--} annihilation fraction (as defined in Ref. [26]), like the $K_S K_L$ channel.

5.2.3. Evaluation of the $\phi\pi^0$ branching ratio

Although we know that, as a general trend, the fraction P_T of P-wave annihilations increases while decreasing the target density, its value in NTP gas and in liquid are not known in a model independent way [24–26]. In particular, the assumption that the quantities F_{Ti} are target independent is made (see Section 5). The analysis of many data of Ref. [32] leads to $P_{\rm NTP} = (52.8 \pm 4.9)\%$ and to $P_L = (8.5 \pm 1.5)\%$, in agreement with the predictions of a cascade model [20]. The above $P_{\rm NTP}$ value has been confirmed by a later evaluation based on the measurements of the $\pi^0\pi^0$ and $\pi^+\pi^-$ production rates both obtained in NTP gas [27]. Instead, the above P_L value is in strong disagreement with the result of an analysis based on the measurement of the $\pi^0\pi^0$ production rate in liquid target (28.8%, Ref. [33]).

In order to get an indicative estimation of the $\phi\pi^0$ branching ratio, we also use the above assumptions. Therefore, assuming $P_{\rm NTP} = (52.8 \pm 4.9)\%$ and $R_{\rm NTP}(\phi\pi^0) = R_{\rm NTPS}(\phi\pi^0) = (2.46 \pm 0.23 \pm 0.07) \times 10^{-4}$ from Eq. (1) we obtain

$$\mathrm{BR}_S^{\rm NTP}(\phi\pi^0) = (5.22 \pm 0.48 \pm 0.56) \times 10^{-4}.$$

This value is higher than that given by the Asterix Collaboration [2], $(4.0 \pm 0.8) \times 10^{-4}$. The difference is not casual. Indeed, in Ref. [2] the S-wave branching ratio is deduced combining measurements in the NTP gas target (with and without L X-rays in coincidence) with the rate value in the liquid target from Ref. [10], which is smaller than that obtained recently by Ref. [31]: $(3.0 \pm 1.5) \times 10^{-4}$ against $(5.5 \pm 0.7) \times 10^{-4}$. Our branching ratio value is more consistent with the higher rate value.

5.3. $K^+K^-\eta$ analysis

5.3.1. Evaluation of $N_{\phi\eta}$ and of $R_{NTP}(\phi\eta)$

The evaluation of the $\phi\eta$ production rate is more elaborate than that of $\phi\pi^0$ because of the poorer statistics and the need of subtracting a background due to phase space $K^+K^-\eta$ or $\phi\pi^0\pi^0$ events from the ϕ peak (see Sections 3.4 and 3.6). We have followed different procedures (based on the study of momentum distributions and missing mass distributions) which have led to consistent results. Therefore we restrict ourselves to schematically describe only one of them.

According to Section 3.6, in order to evaluate the number of $\phi\eta$ ($N_{\phi\eta}$) we have used momentum distributions. Anyway, instead of distributions vs. p_T (which are projections on the p_T axis of Fig. 4a), we have used projections on the η line in the same figure. That is, we have distributed the difference $\Delta p_T = p_T(\text{exp}) - p_T(\text{th})$, where $p_T(\text{exp})$ is the measured p_T value of a particular event and $p_T(\text{th})$ is the total momentum evaluated by the p_T–m_{KK} relation of Section 4 using the measured value of m_{KK} and $m_X = m_\eta$ (see the example of Fig. 18). In Fig. 4a, Δp_T measures the separation along a vertical line of an experimental momentum value from the theoretical η curve. In these distributions η events accumulate in a narrow peak around 0 GeV/c superimposed on a smooth background; the peak width is quite independent of the m_{KK} interval.

According to this, we have built up the distributions vs. Δp_T for events belonging to two different m_{KK} intervals (labelled 1 and 2), one including the ϕ peak (for instance, $1.01 < m_{KK} < 1.03$ GeV/c^2, Fig. 18) the other excluding it (for instance, $m_{KK} > 1.04$ GeV/c^2). We have fit the distributions in the intervals around the η peak with a gaussian plus a third order polynomial in order to obtain the numbers of the peak events,

$$N_1 = N_{\phi\eta} + N_1(\text{KK}\eta),$$

$$N_2 = N_2(\text{KK}\eta).$$

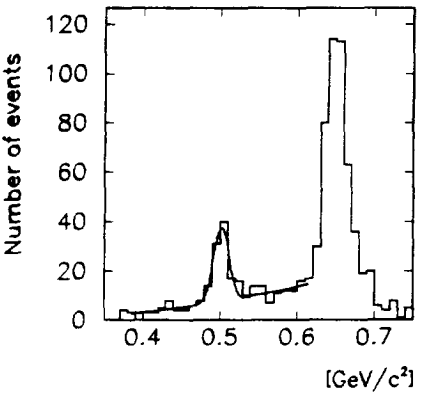

Fig. 18. Δp_T distribution for $K^+K^-\eta$ events with $1.01 < m_{KK} < 1.03$ GeV/c^2 (see text). On the abscissa the values of the quantity $\Delta p_T + p_\phi$ are given, where $p_\phi = 0.5$ GeV/c^2 is the ϕ momentum in the $\phi\eta$ final state.

For the sake of estimating the unknown quantity $N_1(\mathrm{KK}\eta)$, and consequently the quantity $N_{\phi\eta}$, we have resorted to Monte Carlo simulations. That is, we have repeated the preceding work on phase space $\mathrm{K^+K^-}\eta$ events and carried out for the same m_{KK} intervals the relevant numbers of peak events,

$$N_{1\mathrm{MC}} = N_{1\mathrm{MC}}(\mathrm{KK}\eta),$$

$$N_{2\mathrm{MC}} = N_{2\mathrm{MC}}(\mathrm{KK}\eta).$$

$N_1(\mathrm{KK}\eta)$ has been evaluated by the relation

$$N_1(\mathrm{KK}\eta) = N_{1\mathrm{MC}}(\mathrm{KK}\eta)\frac{N_2(\mathrm{KK}\eta)}{N_{2\mathrm{MC}}(\mathrm{KK}\eta)}.$$

We have repeated the analysis for 1 and 2 intervals with different widths obtaining consistent results. Moreover, by comparing experimental and Monte Carlo $\mathrm{K^+K^-}\eta$ distributions for $m_{\mathrm{KK}} > 1.04\ \mathrm{GeV}/c^2$ we have ascertained that $\mathrm{K^+K^-}\eta$ events have a phase space behaviour.

As a final result we have

$$N_{\phi\eta} = 52 \pm 16.$$

The error includes all effects due to statistics, best fit procedures and Monte Carlo simulations. To give an indication of the amount of $\mathrm{K^+K^-}\eta$ events we report that in the m_{KK} interval $1.01-1.03\ \mathrm{GeV}/c^2$ it turns out that $N_1 = 74.5 \pm 15.3$ and $N_1(\mathrm{KK}\eta) = 22.3 \pm 3.0$.

Finally, we calculate the $\phi\eta$ production rate. For this aim, we have by Monte Carlo calculations evaluated the efficiencies to detect $\phi\eta$ events produced in S- and P-waves. They are different because of the different angular and momentum distributions of the kaons in the two cases. They are

$$\varepsilon_{\phi\eta\mathrm{S}} = (1.791 \pm 0.064) \times 10^{-2},$$

$$\varepsilon_{\phi\eta\mathrm{P}} = (1.267 \pm 0.055) \times 10^{-2}.$$

As we do not know the annihilation probability in S- and P-waves (see Section 4), according to Eqs. (1) and (2) of Section 5 we give the following lower and upper limits for the production rates in NTP gas assuming all annihilations in S- or in P-wave:

$$R_{\mathrm{NTP}}(\phi\eta) = (0.74 \pm 0.22 \pm 0.03) \times 10^{-4} \quad \text{(lower limit)},$$

$$R_{\mathrm{NTP}}(\phi\eta) = (1.04 \pm 0.33 \pm 0.05) \times 10^{-4} \quad \text{(upper limit)}.$$

The former error is "statistical" (related to $N_{\phi\eta}$) and the latter one is systematic (related to $N_{\bar{\mathrm{p}}}$, ε and $\varepsilon_{\phi\eta\mathrm{X}}$). The true production rate will be somewhere in between; if we assume $P_{\mathrm{NTP}} = 52.8\%$ and $\mathrm{BR}_{\mathrm{S}}^{\mathrm{NTP}}(\phi\eta) = \mathrm{BR}_{\mathrm{P}}^{\mathrm{NTP}}(\phi\eta)$, we obtain the middle value

$$R_{\mathrm{NTP}}(\phi\eta) = (0.87 \pm 0.21) \times 10^{-4}.$$

The $\phi\eta$ production rate has been measured in two other experiments. With a NTP gas target Ref. [2] has measured the value $R_{\mathrm{NTP}}(\phi\eta) = (0.37 \pm 0.09) \times 10^{-4}$; with the same target and with L X-rays in coincidence the same group has obtained the value

$(0.41 \pm 1.6) \times 10^{-4}$, practically equal to that without X-ray coincidence. Both these values are about one half our middle value. Ref. [3] gives the value $(0.66 \pm 0.19) \times 10^{-4}$ with a liquid target.

Although the data are affected by large errors and those in gas are not consistent, we may draw a qualitative conclusion. That is, the similarity of the rates with and without L X-ray coincidence of Ref. [2] and the higher value found by us in gas compared with that found in a liquid target suggests that the P-wave contribution could not be negligible in the $\phi\eta$ production, as in the $\phi\pi^0$ case.

5.3.2. $K^+K^-\eta$ production rate

The previous analysis has shown that the experimental distribution of the $K^+K^-\eta$ events is phase space like and has allowed us to evaluate the relevant production rate. For a total number of events ($\phi\eta$ excluded) $N_T(KK\eta) = 847 \pm 61$ and a detection efficiency $\varepsilon = 2.27\%$, the production rate turns out to be

$$R_{NTP}(KK\eta) = (4.67 \pm 0.35) \times 10^{-4}.$$

This value cannot be compared to previous data, at least to our knowledge.

5.3.3. Estimate of the $\phi\eta$ branching ratios

Eq. (2) contains the three unknown quantities P_T, $BR_S^{NTP}(\phi\eta)$ and $BR_P^{NTP}(\phi\eta)$. If we use the value $P_{NTP} = (52.8 \pm 4.9)\%$ with the cautions stressed in Section 5.2.3, we obtain a linear relation between $BR_S(\phi\eta)$ and $BR_P(\phi\eta)$:

$$BR_S^{NTP}(\phi\eta) = 1.567 \times 10^{-4} - 0.791 BR_P^{NTP}(\phi\eta), \tag{3}$$

with the following limits for the branching ratios in pure S- and P-waves:

$$BR_S^{NTP}(\phi\eta) \leqslant (1.57 \pm 0.49) \times 10^{-4},$$

$$BR_P^{NTP}(\phi\eta) \leqslant (1.97 \pm 0.65) \times 10^{-4}.$$

Eq. (3) is plotted in Fig. 19, where also the experimental uncertainties are indicated by the errors on the maximum values of the branching ratios (systematic and statistical errors are added quadratically).

We can write an equation like Eq. (3) also for the case of a liquid target. For this aim, we consider Eq. (1) and assume $P_L = (8.5 \pm 1.5)\%$ (see Section 5.2.3). $R_L(\phi\eta)$ can be estimated by the ratio $R_L(\phi\pi^0)/R_L(\phi\eta) = 8.3 \pm 1.7 \pm 1.3$ [34] and by the $R_L(\phi\pi^0)$ value measured in a liquid target: $(5.5 \pm 0.7) \times 10^{-4}$ (Ref. [31]; we neglect the value [10] $(3.0 \pm 1.5) \times 10^{-4}$ because of its large error). It turns out that $R_L(\phi\eta) = (0.66 \pm 0.19) \times 10^{-4}$ and

$$BR_S^L(\phi\eta) = 0.721 \times 10^{-4} - 0.073 BR_P^L(\phi\eta). \tag{4}$$

Now, according to the usual assumptions, we make the approximation $BR_i^L = BR_i^{NTP} = BR_i$. Then Eqs. (3) and (4) form a linear system of two equations and two unknowns which is resolved graphically in Fig. 19. The solution is

$$BR_S(\phi\eta) = (0.64 \pm 0.25) \times 10^{-4},$$

$$BR_P(\phi\eta) = (1.18 \pm 0.84) \times 10^{-4}.$$

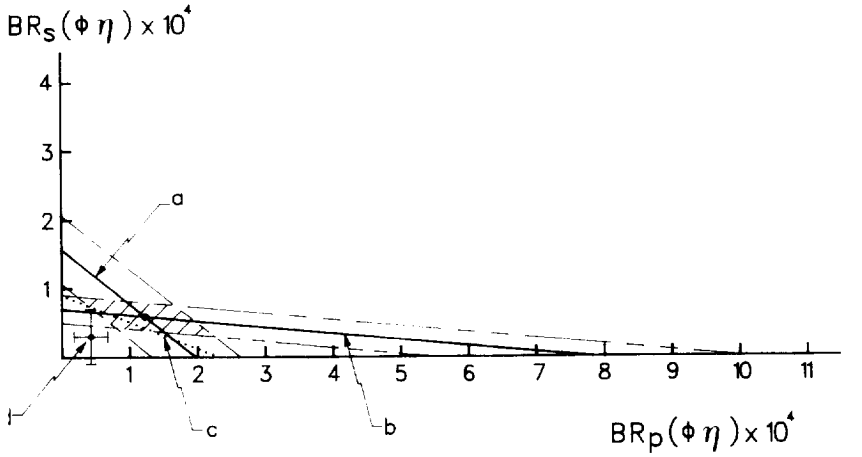

Fig. 19. BR_S vs. BR_P for $\phi\eta$ production (see Section 5.3.1). (a) Gas target at NTP. (b) Liquid target and $P_L = 8.5\%$; (c) Liquid target and $P_L = 28.8\%$. (d) Values of BR_S and BR_P from Ref. [2]. The coordinates of the intersection of the lines (a) and (b) give the values of BR_S and BR_P; the dashed area around the intersection estimates the uncertainties on the branching ratios.

The errors are obtained from Fig. 19. These values are higher than those of Ref. [2] (see Fig. 19).

Finally, if we use for P_L the value 28.8% following Ref. [33], we obtain the dotted straight line in Fig. 19 instead of the line according to Eq. (4). The intersection of this line with that from the gas target emphasises BR_P and depresses BR_S.

5.4. Results from data collected without a slow particle trigger

The main features of the data collected without the slow particle trigger (Section 2) are shown by the Dalitz plot and the m_{KK} distribution of Fig. 20. Notice that the event distribution in this Dalitz plot is complementary to that of Fig. 6b, as a consequence of

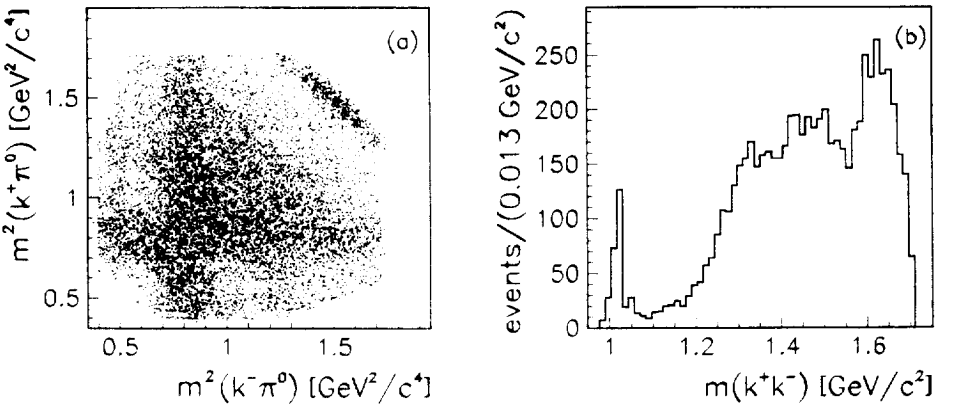

Fig. 20. Data collected without slow trigger. (a) Dalitz plot. (b) K^+K^- invariant mass distribution for $K^+K^-\pi^0$ events.

the different trigger operations; that is, in Fig. 20a the high value region of the KK invariant mass is more populated than that of small values. A preliminary Dalitz plot analysis has shown that the P-wave contribution to the $\phi\pi^0$ production is negligible ($< 8\%$ at 95% C.L.). The analysis of the KK invariant mass distribution has led to the following number of events, efficiency and rate:

$$N_{\phi\pi^0} = 196 \pm 24,$$

$$\varepsilon_{\phi\pi^0 S} = (8.92 \pm 0.16) \times 10^{-2},$$

$$R_{NTPS}(\phi\pi^0) = (2.58 \pm 0.39) \times 10^{-4},$$

the last of which is in good agreement with the value obtained with the slow particle trigger, $(2.46 \pm 0.23 \pm 0.07) \times 10^{-4}$.

The $K^+K^-\eta$ statistics turns out to be high enough in spite of the worse trigger conditions for such events; actually, we have evaluated $N(KK\eta) = 425 \pm 42$ corresponding to a production rate $R_{NTP} = (4.61 \pm 0.47) \times 10^{-4}$, in good agreement with the slow trigger case. On the contrary, the $\phi\eta$ statistics is very poor ($N_{\phi\eta} = 17.4 \pm 8.7$). Nevertheless, we have estimated lower and upper limits for the production rate in NTP gas in agreement with the values found previously:

$$R_{NTP}(\phi\eta) = (0.83 \pm 0.41) \times 10^{-4} \quad \text{(lower limit)},$$

$$R_{NTP}(\phi\eta) = (1.21 \pm 0.61) \times 10^{-4} \quad \text{(upper limit)}.$$

They have been evaluated by assuming annihilations only in S- or in P-wave.

6. Summary and final remarks

We have measured the production rates of the $\phi\pi^0$, $\phi\eta$ and $K^+K^-\eta$ final states in the annihilation of stopped antiprotons in a hydrogen gas target at NTP conditions and deduced the branching ratios. Our results are collected and compared to data from other experiments in Table 1 and Fig. 19. In the following, their main features are summarised and some physical consequences are shown.

6.1. $\phi\pi^0$ production rate

By analysing the angular distribution of the kaons produced by the ϕ decay we have ascertained that $\phi\pi^0$ is produced essentially in S-wave with a P-wave production rate compatible with zero. This result is in good agreement with that obtained by the Asterix Collaboration [2] with different procedures.

6.2. $\phi\eta$ and $K^+K^-\eta$ production rate

The acceptance of our apparatus for the decay angular distribution of the charged kaons is too limited in the $\phi\eta$ channel and does not permit to resolve the contributions

from the $^3S_1$ and $^1P_1$ initial states. For this reason, for the $\phi\eta$ production rate only lower and upper limits could be obtained, with a middle value of $(0.87 \pm 0.21) \times 10^{-4}$. This value is about twice as high as the Asterix one [2] obtained at the same target density, and the two values are compatible with low probability. The analysis has shown also that $K^+K^-\eta$ events are distributed according to phase space and the relevant production rate has been evaluated, $(4.67 \pm 0.35) \times 10^{-4}$. To our knowledge, no previuos result on this reaction exists. Anyway, it turns out to be twice as high as the $K_SK_S\eta$ production rate measured in a liquid target ($(2.3 \pm 0.7) \times 10^{-4}$, quoted in Ref. [35]).

6.3. Branching ratios

The S- and P-wave branching ratios for the $\phi\pi^0$ and $\phi\eta$ production have been derived in a model dependent way. As only the S-wave contribution has been observed, the evaluation of the $\phi\pi^0$ branching ratio is straightforward. Our result is somewhat higher than that deduced in Ref. [2] with a wholly different procedure and is consistent with the recent rate value in liquid given in Ref. [31]. The value 52.8% has been assumed for the fraction of P-wave annihilations.

In order to estimate the $\phi\eta$ branching ratios in S- and P-waves we have combined through Eq. (1) our $\phi\eta$ production rate in NTP hydrogen gas, the $\phi\pi^0$ production rate obtained with a liquid target by Ref. [31] and the ratio $R_L(\phi\pi^0)/R_L(\phi\eta)$ measured in a liquid target by Ref. [34]. We have assumed that the branching ratios as defined in Section 5 are target independent and that the P-wave fraction of annihilations in a liquid target is 8.5%, according to Ref. [32]. It turns out that the branching ratio is higher in P-wave than in S-wave. Our values are 2–3 times higher than those obtained in Ref. [2].

6.4. OZI rule

Using our preliminary result [36] of the measurement of the $\omega\pi^0$ production rate for annihilations in gas,

$$R_{NTP}(\omega\pi^0) = (19.1 \pm 4.7) \times 10^{-4},$$

the ratio

$$W = R_{NTP}(\phi\pi^0)/R_{NTP}(\omega\pi^0) = (129 \pm 35) \times 10^{-3}$$

is obtained, which is significantly higher than the OZI rule prediction from ($W \approx 4.2 \times 10^{-3}$, see Section 1). So we confirm the strong violation of the OZI rule seen in Refs. [2–5] for the annihilations of low energy antinucleons.

As the phase space factor F is close to 1 (see Section 1), the high value of the ratio $\phi\pi^0/\omega\pi^0$ cannot be explained as a simple kinematical effect. The fact that the reaction $\bar{p}p \to \phi\pi^0$ comes mainly from the S-wave indicates a strong dependence of the ϕ production on the quantum numbers of the initial state. Bearing in mind that the S-wave annihilation into the $\phi\pi^0$ final state is possible only from the spin triplet state $^3S_1$, whereas the P-wave annihilations come only from the singlet state $^1P_1$, we may

formulate the above mentioned fact as a dynamical selection rule of the dominance of the spin triplet state in the ϕ production. This rule has a natural explanation in the model of polarised intrinsic strangeness of the nucleon [17].

The data to evaluate the ratio $W = R(\phi\eta)/R(\omega\eta)$ are uncertain. For the $\phi\eta$ production rate there is only a value in a liquid target [3,31,34]: $(0.66 \pm 0.19) \times 10^{-4}$. Assuming $P_L = 8.5\%$, Ref. [34] estimates the value at $(0.48 \pm 0.17) \times 10^{-4}$. Using the branching ratios given by Ref. [2], a smaller value is found. For the $\omega\eta$ production, three measurements in a liquid target are known: $(104 \pm 10) \times 10^{-4}$ [37], $(151 \pm 12) \times 10^{-4}$ [38] and $(46 \pm 14) \times 10^{-4}$ [39]. These values are not all consistent; in spite of this, one can conclude that the ratio $W = R_L(\phi\eta)/R_L(\omega\eta)$ is small and close to the value predicted by the OZI rule (of the order of 10^{-3}). We stress that this evaluation of W concerns essentially S-wave annihilations. The same conclusion has been reached by Ref. [2].

The features of the production of ϕ associated with η (P-wave dominance and respect for the OZI rule in S-wave annihilations) appear to be different from those of the production of ϕ associated with π^0. This fact should be clarified by further experimental and theoretical investigations, which could underline a different behaviour of the $\phi\eta$ production related to the presence of a non-negligible $\bar{s}s$ component in the η-meson [17].

Acknowledgements

The members of the Pavia group thank the technical staffs of the Dipartimento di Fisica Nucleare and Teorica of the Pavia University and of the Istituto Nazionale di Fisica Nucleare, Sezione di Pavia for the active collaboration in the different stages of the Obelix activity. They like to name with gratitude C. Marciano, who planned the support structure of the central part of the apparatus and the beam pipe and carried them out taking advantage of the ability and experience of S. Bricola, L. Cecco, T. Locatelli and A. Vicini; this staff has also given continuous assistance during all the data collection runs. Particular thanks are due to C. Casella, who has managed with high efficiency our precious piles of tapes, and to R. Cecco, for his appreciated collaboration in the management of the computer system of the experiment.

The JINR group acknowledges the support by the grant ML9300 from the International Science Foundation and Russian Government.

References

[1] S. Okubo, Phys. Lett. B 5 (1963) 165;
G. Zweig, CERN report No. 8419/TH412 (1964);
I. Iizuka, Prog. Theor. Phys. Suppl. 37 38 (1966) 21.
[2] J. Reifenroether et al., Phys Lett. B 267 (1991) 229.
[3] M.A. Faessler, Proc. NAN-93 Conf., Moscow 1993, Yad. Fiz. 57 (1994) 1764;
P. Blum, preprint IEKP-KA/94-12; invited talk at 6th Int. School of Physics of exotic atoms, Erice 1994.

[4] V.G. Ableev et al., Phys. Lett. B 334 (1994) 237.
[5] V.G. Ableev et al., Nucl. Phys. A 585 (1995) 577.
[6] Review of Particle Properties, Phys. Rev. D 50 (1994) 1175.
[7] S. Okubo, Phys. Rev. D 16 (1977) 2336.
[8] A.M. Cooper et al., Nucl. Phys. B 146 (1978) 1.
[9] M.G. Sapozhnikov, Proc. LEAP-94 Conf., Bled 1994; JINR preprint E15-94-501, Dubna (1994).
[10] M. Chiba et al., Phys. Rev. D 38 (1988) 2021.
[11] C.B. Dover and P.M. Fishbane, Phys. Rev. Lett. 62 (1989) 2917.
[12] M.P. Locher, Y. Lu and B-S. Zou, Z. Phys. A 347 (1994) 281.
[13] D. Buzatu and F. Lev, Phys. Lett. B 329 (1994) 143.
[14] M.P. Locher and Y. Lu, preprint PSI-PR-94-28, Villigen (1994).
[15] D. Buzatu and F. Lev, JINR preprint E4-94-158, Dubna (1994).
[16] J. Ellis, E. Gabathuler and M. Karliner, Phys. Lett. B 217 (1989) 173.
[17] J. Ellis et al., preprint CERN-TH.7326/94, Geneva (1994).
[18] A. Adamo et al. Sov. J. Nucl. Phys. 55 (1992) 1732.
[19] A. Adamo et al., Phys. Lett. B 285 (1992) 15.
[20] G. Reifenroether and E. Klempt, Nucl. Phys. A 486 (1989) 885.
[21] G. Reifenroether at al., Phys. Lett. B 214 (1988) 325.
[22] A. Adamo et al., Nucl. Phys. A 569 (1994) 761.
[23] V. Filippini et al., Phys. Rev. D 51 (1995) 2247.
[24] U. Gastaldi, Nucl. Phys. B 23 (1991) 224; in: Exotic atoms and molecules and their interactions, INFN/AE 94/24, p. 85.
[25] A. Rotondi, Nucl. Phys. A 558 (1993) 235c; in: Exotic atoms and molecules and their interactions, INFN/AE 94/24, p. 251.
[26] U. Gastaldi et al., Phys. Lett. B 320 (1994) 193.
[27] M. Agnello et al., Phys Lett. B 337 (1994) 226.
[28] J. Riedelberger et al., Phys. Rev. C 40 (1989) 2717.
[29] C. Ghesquiere, Symp. on Antinucleon–nucleon interaction, Liblice 1974; CERN 74-18, p. 486.
[30] J.D. Jackson, Nuovo Cimento 34 (1964) 1644.
[31] C. Amsler et al., Phys. Lett. B, in press.
[32] J. Reifenroether and E. Klempt. Phys. Lett. B 245 (1990) 129.
[33] C. Amsler et al., Phys. Lett. B 297 (1992) 214.
[34] C. Amsler et al., Phys. Lett. B 319 (1993) 37.
[35] R. Armenteros and B. French, High energy physics, ed. E.H.S. Burhop, Vol. IV (Academic, London, 1969) p. 237.
[36] A. Zoccoli et al., Proc. LEAP-94 Conf., Bled 1994.
[37] L. Adiels et al., Z. Phys. C 42 (1989) 49.
[38] C. Amsler et al., Z. Phys. C 58 (1993) 175.
[39] M. Chiba et al., Phys. Rev. D 39 (1989) 3227.